Time Dependence of Few-Body Förster Interactions among Ultracold Rydberg Atoms

Zhimin Cheryl Liu,[1,2] Nina P. Inman,[1] Thomas J. Carroll,[3] and Michael W. Noel[1]
[1]Department of Physics, Bryn Mawr College, Bryn Mawr, Pennsylvania 19010, USA
[2]Department of Physics, University of Colorado, Boulder, Colorado 80309, USA
[3]Department of Physics and Astronomy, Ursinus College, Collegeville, Pennsylvania 19426, USA

(Received 24 November 2019; accepted 17 March 2020; published 31 March 2020)

Rubidium Rydberg atoms in either $|m_j|$ sublevel of the $36p_{3/2}$ state can exchange energy via Stark-tuned Förster resonances, including two-, three-, and four-body dipole-dipole interactions. Three-body interactions of this type were first reported and categorized by Faoro *et al.* [Nat. Commun. **6**, 8173 (2015)] and their Borromean nature was confirmed by Tretyakov *et al.* [Phys. Rev. Lett. **119**, 173402 (2017)]. We report the time dependence of the N-body Förster resonance $N \times 36p_{3/2,|m_j|=1/2} \rightarrow 36s_{1/2} + 37s_{1/2} + (N-2) \times 36p_{3/2,|m_j|=3/2}$, for $N = 2$, 3, and 4, by measuring the fraction of initially excited atoms that end up in the $37s_{1/2}$ state as a function of time. The essential features of these interactions are captured in an analytical model that includes only the many-body matrix elements and neighboring atom distribution. A more sophisticated simulation reveals the importance of beyond-nearest-neighbor interactions and of always-resonant interactions.

DOI: 10.1103/PhysRevLett.124.133402

Understanding few-body and many-body interactions is of near universal importance, with relevance to problems in atomic, condensed matter, and nuclear physics. Experiments with ultracold atoms and molecules have significantly advanced that understanding. For example, the spin lattice that forms when polar molecules are confined with an optical lattice may be useful in modeling quantum magnetism and topological insulators [1,2]. Precise control over the interactions in systems of ultracold atoms has recently been realized in a variety of experiments. The few-body universal quantum states predicted by Efimov [3] have been observed and studied extensively in ultracold gases [4,5]. Progress with dipolar quantum gases includes the observation of stable quantum droplets in a dysprosium Bose-Einstein condensate [6], the observation of angular oscillations of quantum droplets, analogous to the behavior of nuclei, induced by the dipole-dipole interaction [7], and the discovery of a regime with supersolid properties [8].

Dipole-dipole mediated energy exchange in an amorphous ultracold Rydberg gas has been studied extensively over the past two decades [9,10]. Precise line shape measurements have contributed to our understanding of the importance of many-body and always resonant exchange in this system [11–15]. Recently, resonant energy transfer between Rydberg atoms and polar molecules has also been observed [16,17].

Less attention has been given to the time evolution of resonant energy exchange in this system. A Ramsey interferency measurement was used to explore dephasing due to always resonant processes [18]. Rabi oscillations in the energy exchange between a pair of isolated atoms has been seen [19,20] along with energy exchange between two well-separated macroscopic samples [21]. Computational and experimental results that image the time dependence of the energy exchange hint at the possibility of localization in this system [22–24]. Using a microwave field to initiate a quantum quench, Orioli *et al.* have explored relaxation of an ultracold Rydberg gas [25]. Further exploration of the time evolution of energy exchange in ultracold Rydberg gases may ultimately shed light on many-body localization and thermalization that complements recent work in other spin systems [26–28].

Resonant few-body dipole-dipole interactions with Rydberg atoms were discovered and studied only recently. Gurian *et al.* observed a four-body resonant interaction in cesium that lies between, and relies on, a pair of two-body interactions [29]. Faoro *et al.* reported on a simpler three-body process in cesium and developed a theory for a class of similar few-body interactions applicable to many Rydberg atoms [30]. More recently, Tretyakov *et al.* observed the same type of three-body interaction in rubidium Rydberg atoms while conclusively demonstrating the Borromean nature of the energy exchange [31]. Additional work has studied coherence of this interaction and its suitability for use in a quantum gate [32,33].

In this Letter, we report on the time dependence of the two-, three-, and four-body dipole-dipole interactions in rubidium

$$p + p \rightarrow s + s', \tag{1}$$

$$p + p + p \rightarrow s + s' + p', \tag{2}$$

$$p + p + p + p \rightarrow s + s' + p' + p', \tag{3}$$

where the state labels have been abbreviated $p = 36p_{3/2,|m_j|=1/2}$, $s = 37s_{1/2}$, $p' = 36p_{3/2,|m_j|=3/2}$, and $s' = 36s_{1/2}$. We present a simple model of the time evolution that is able to approximately describe the shape of the time-dependence curve, though it neglects always-resonant and beyond-nearest-neighbor interactions. In contrast, a full many-body simulation matches the experiment more closely, revealing the importance of these physical processes.

The resonant interactions of Eqs. (1)–(3) are indicated by solid arrows in the Stark map of Fig. 1(a). The two-body exchange is resonant at an electric field of 3.29 V/cm. Tuning to higher field introduces an energy defect that is equal to $E_p - E_{p'}$ at 3.52 V/cm. A third p atom can account for the defect via either of the equally detuned two-body exchanges $p + s' \rightarrow s' + p'$ or $p + s \rightarrow s + p'$. Similarly, the energy defect is $2(E_p - E_{p'})$ at 3.80 V/cm which requires a fourth p atom. One example of the many possible four-body interactions is shown in Fig. 1(b). While the few-body energy exchange can be perturbatively calculated as a sequence of two-body interactions, it is essentially Borromean in nature and requires all atoms to participate simultaneously [31]. More Förster resonances following this pattern are possible and are discussed in Ref. [30].

In our experiment, about 10^6 ^{85}Rb atoms are trapped in a magneto-optical trap (MOT) of diameter ≈0.5 mm. The trapping laser at 780 nm cycles atoms between the $5s$ and $5p$ states. A 776 nm laser drives the $5p$ to $5d$ transition and a 1265 nm laser excites atoms to the $36p$ state. Simulation suggests a Rydberg density on the order of 10^8 cm^{-3}, corresponding to an average spacing of about 20 μm. Highly excited atoms then exchange energy through a dipole-dipole interaction and the fraction of atoms in each state is quantified using directed field ionization (DFI) [34].

A set of coaxial cylinders placed on either side of the MOT allow us to apply static and time varying electric fields [35]. To separate the p and p' states, atoms are excited in an electric field of 4.2 V/cm. The interaction pulse, which is a square voltage pulse whose length and amplitude can be varied, is then applied to one cylinder.

To determine the strength of this energy exchange, we measure the fraction of atoms that end up in the s state. The time-resolved field ionization signals from the s and p states obtained using standard selective field ionization (SFI) are almost completely overlapping. In addition, the p-state signal causes ringing in our detector, which makes quantitative measurement of the s'-state fraction difficult. We therefore use DFI to better resolve the s and p states and measure the s-state fraction [34–36]. Using a genetic algorithm, DFI optimizes a small perturbation that is added to an SFI ramp. This perturbation directs a fraction of the s-state signal along a pathway through the Stark map that ionizes early in time relative to that of the p-state signal, allowing us to quantify the fraction of atoms that

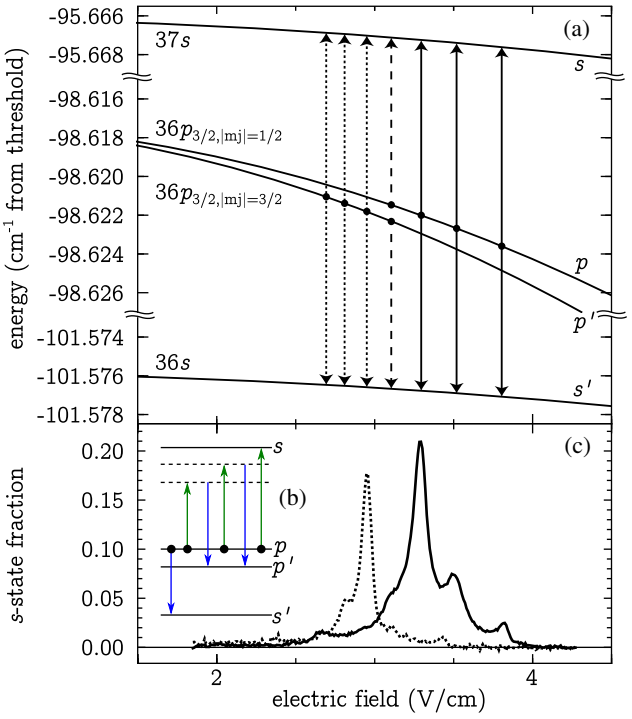

FIG. 1. (a) Stark map showing the s, p, s', and p' energy levels as a function of electric field. Solid arrows correspond to Förster resonances for which the time dependence was studied, with atoms are initially excited to the p state. Dotted lines are the complementary set of resonances for an initial state of all p' atoms. The dashed line is the location of the two-body $p + p' \rightarrow s + s'$ resonance. (b) Energy level diagram of a possible four-body interaction of Eq. (3). (c) Experimental s-state fraction as a function of electric field for an initial state composed of p atoms (solid line) or p' atoms (dotted line).

end up in the s state. During optimization of the DFI perturbation, the delay between excitation and the start of the field ionization ramp is set to zero and no interaction pulse is present. After optimization we add a fixed delay of 10 μs between excitation and DFI to provide room for an interaction pulse of varying amplitude and/or length. During this 10 μs window, blackbody radiation can drive transitions to neighboring states. This leads to a constant 1.5% transfer to the s state in the absence of any dipole-dipole interaction, which we subtract from our dipole-dipole fraction measurements.

With the width of the interaction pulse fixed at 9 μs, we scan the amplitude to tune various interactions into resonance. We alternate between exciting the p and p' states and average several thousand shots for each amplitude. For a sample excited to the p state, the fraction of atoms that end up in the s state is shown in Fig. 1(c) by the solid line. In this scan we can clearly identify two-, three-, and four-body resonant energy exchanges. We also see a feature at the location of the $p + p' \rightarrow s + s'$ resonance, which is marked by the dashed arrows in Fig. 1(a). We associate this with an off-resonant energy exchange. First the off-

resonant $p + p \rightarrow s + s'$ populates the $s + s'$ state. From this state, the resonant $s + s' \rightarrow p + p'$ can proceed. In contrast to the resonant few-body interactions studied here, this is an inefficient off-resonant multistep process that seeds the $p + p' \rightarrow s + s'$ exchange.

Other features in the signal have yet to be understood. In particular, we see a broad tail to the low field side of the two-body exchange along with the small peak near 2.7 V/cm. The dotted lines in Figs. 1(a) and 1(c) show the complementary set of resonances that occur with initial excitation to the p' state. The field axis is calibrated by fitting the locations of the two-body resonances. We check this calibration by measuring the splitting between the p and p' states. These two calibrations agree to within 5%.

We have also investigated the time dependence of the two-, three-, and four-body interactions. To collect this data, we scan the time that the interaction field is applied for each of the three resonant fields at 3.29, 3.52, and 3.80 V/cm. The fraction of atoms in the s state as a function of time is shown by the solid lines in Fig. 2 for each of these three fields. The primary uncertainty in the s-state fraction is due to systematic errors in calibration of about 5%. This is larger than the statistical error since we average over thousands of shots at each time.

For two atoms at fixed separation, the time dependence should be given by Rabi oscillations; in fact, Ravets *et al.* have observed Rabi oscillations between a pair of Rydberg atoms [20]. A more complicated, but still coherent, oscillation is expected for few-body interactions in a close triplet or quadruplet [33]. However, we have a different amorphous sample of atoms on each shot of our laser, which averages out the oscillations. The early time behavior of Fig. 2 is dominated by high frequency oscillations among closely spaced atoms, which drive the relatively rapid increase in s-state fraction. This is followed by a gradual approach to saturation due to more distant interactions.

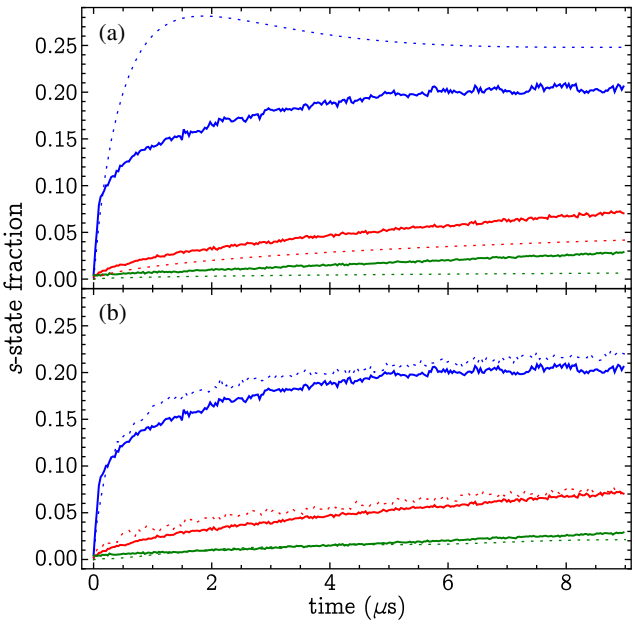

FIG. 2. Fraction of atoms in the s state as a function of interaction time for (a) the experiment (solid) compared to the simple analytical model (dashed) and (b) the experiment (solid) compared to the simulation (dashed). The two-, three-, and four-body interactions are shown in blue, red, and green, respectively. In (a), a density of 9.5×10^7 cm^{-3} was chosen for the simple model to match the initial slope of the two-body interaction. In (b), the simulations were run at a density of 2.4×10^8 cm^{-3}.

We can begin to understand the shape of the time dependence curves for the N-body interactions by considering three main factors. First, as N increases, the saturation level of the population transfer decreases so that one expects the s-state fraction to eventually plateau at 0.25, $0.1\bar{6}$, and 0.125 for $N = 2$, $N = 3$, and $N = 4$, respectively. Second, the matrix elements decrease as N increases since each additional two-body step brings in another factor of the detuning. This is, however, somewhat mitigated by the increasing number of paths from initial state to final state as N increases. Finally, in an amorphous sample of atoms the distance between a close pair will be less than the average distance among close triplets or quadruplets.

We construct a simple analytical model comprised of these three factors. We assume that the N-body interaction is dominated by contributions from clusters of N atoms. The jth-nearest neighbor probability distribution is given by

$$g(r_{0j}|r_{0(j-1)}) = 4\pi r_{0j}^2 \rho e^{-(4/3)\pi\rho(r_{0j}^3 - r_{0(j-1)}^3)}, \tag{4}$$

where r_{0j} is the distance from the central atom to its jth-nearest neighbor and ρ is the Rydberg atom density [37,38]. Beyond-nearest-neighbor atoms may be closer to each other than to the central atom. Since the r^{-3} dependence of the dipole-dipole interaction lends much greater weight to closely spaced atoms and $r_{(i\geq 1)j}$ could be significantly less than r_{0j}, we average over the distances $r_{(i\geq 1)j}$.

The matrix elements can be calculated perturbatively by summing over all paths from the initial state $|i\rangle$ to the final state $|f\rangle$ with

$$\omega_2 = \frac{\langle f|\hat{\sigma}_{fi}|i\rangle}{r_{fi}^3}, \tag{5}$$

$$\omega_3 = \sum_j \frac{\langle f|\hat{\sigma}_{fj}|j\rangle\langle j|\hat{\sigma}_{ji}|i\rangle}{\delta_j r_{fj}^3 r_{ji}^3}, \tag{6}$$

$$\omega_4 = \sum_j \sum_k \frac{\langle f|\hat{\sigma}_{fj}|j\rangle\langle j|\hat{\sigma}_{jk}|k\rangle\langle k|\hat{\sigma}_{ki}|i\rangle}{\delta_j \delta_k r_{fj}^3 r_{jk}^3 r_{ki}^3}, \tag{7}$$

where $|j\rangle$ and $|k\rangle$ are intermediate states, δ_j is the detuning of the jth intermediate state, and $\hat{\sigma}_{ij}$ is the operator that takes the jth state to the ith state. Since the dipole-dipole

interaction couples pairs of atoms, each operator $\hat{\sigma}$ represents a product of single-atom operators that take an individual atom from an s state to a p state or vice versa [23,39].

For this simple model, we ignore the angular dependence and simply multiply the summands in Eqs. (6) and (7) by the total number of possible paths from a given initial to a given final state. We also consider δ to be fixed for every step, yielding

$$\omega_2 = \frac{\mu\nu}{r_{12}^3}, \qquad \omega_3 = \frac{2(\mu\nu)^2}{\delta r_{12}^3 r_{23}^3}, \quad \text{and} \quad \omega_4 = \frac{16(\mu\nu)^3}{\delta^2 r_{12}^3 r_{23}^3 r_{34}^3}, \tag{8}$$

where $\mu \approx 700\, ea_0$ and $\nu \approx 600\, ea_0$ are the transition dipole moments p or $p' \to s$ and p or $p' \to s'$, respectively. There are significantly more paths from initial to final state if $\pm m_j$ states are included.

The time dependence of the population transfer to the s state among a cluster of N atoms should be oscillatory with frequencies similar to ω_N and an amplitude determined by the saturation level. Since we average the time dependence over atomic separations, the particular form of the oscillation is not important. We use $(2N)^{-1}\sin^2(\omega_N t)$, where $(2N)^{-1}$ gives the saturation level. The population fractions $P_N(t)$ transferred to the s state are

$$P_2(t) = 2\pi\rho \int_0^\infty e^{-(4/3)\pi\rho r^3} \sin^2\left[\frac{\mu\nu}{r^3} t\right] dr, \tag{9}$$

$$P_3(t) = \frac{16\pi\rho^2}{3} \int_0^R r_{02}^2 e^{-(4/3)\pi\rho r_{02}^3} \int_0^{r_{02}} r_{01}^2 \int_0^\pi \sin^2\left[\frac{(\mu\nu)^2 t}{\delta r_{01}^3 (r_{01}^2 + r_{02}^2 - 2r_{01}r_{02}\cos\theta_{12})^{3/2}}\right] d\theta_{12} dr_{01} dr_{02}, \tag{10}$$

$$P_4(t) = 16\pi\rho^3 \int_0^R r_{03}^2 e^{-(4/3)\pi\rho r_{03}^3} \int_0^{r_{03}} r_{02}^2 \int_0^{r_{02}} r_{01}^2 \int_0^\pi \int_0^\pi \times \sin^2\left[\frac{(\mu\nu)^3 t}{\delta^2 r_{01}^3 (r_{01}^2 + r_{02}^2 - 2r_{01}r_{02}\cos\theta_{12})^{3/2} (r_{02}^2 + r_{03}^2 - 2r_{02}r_{03}\cos\theta_{23})^{3/2}}\right] d\theta_{12} d\theta_{23} dr_{01} dr_{02} dr_{03}, \tag{11}$$

where θ_{ij} is the angle between $\vec{r}_{0i}$ and $\vec{r}_{0j}$ and the numerical prefactor includes the saturation level. The two-body result of Eq. (9) can be integrated analytically [15,40]. The three- and four-body results in Eqs. (10)–(11) must be integrated numerically. The integration is terminated at a radius R large enough that it converges.

The time dependence of Eqs. (9)–(11) is shown by dashed lines in Fig. 2(a). The density was chosen to match the initial slope of the model's two-body time dependence to the experimental data, yielding $\rho = 1.0(0.3) \times 10^8\,\mathrm{cm}^{-3}$. This model captures the essential features of the experimental curves. However, in attempting to match the two-body data, it significantly underpredicts the three- and four-body population transfer. This simple model ignores the fact that the experimental three- and four-body time dependence each include a contribution from the shoulder of the two-body interaction. This could account for some, but not all, of the disagreement.

Our simple model neglects always-resonant interactions and beyond-nearest-neighbor interactions, which have been shown to play a role in the dipole-dipole energy exchange in a three-Rydberg-atom chain [41]. To address these deficiencies, we have also simulated our system by constructing the Hamiltonian matrix using Eqs. (5)–(7) while averaging over the angular dependence [20,42], under the assumption that the Rydberg atoms remain frozen in place for the duration of the experiment. We randomly place 40 atoms in a spherical volume of radius 34 μm, while using the blockade radius to estimate a minimum distance between atoms. We calculate the time evolution by solving the Schrödinger equation on a supercomputer for each atom and its closest 8 neighbors, resulting in a Hamiltonian matrix of rank 48 620. The results are averaged over all 40 atoms and the process is repeated so that a few hundred random instances are averaged. The simulated results, which agree well with the data, are shown by the dashed lines in Fig. 2(b).

Our simulations suggest that our Rydberg density is $2.4(0.1) \times 10^8\ \mathrm{cm}^{-3}$, where the statistical uncertainty was calculated from multiple simulation runs at a range of densities. By averaging over many random arrangements of atoms at this density, we calculate average interaction strengths of $\omega_2 = 162 \pm 6$, $\omega_3 = 1.6 \pm 0.1$, and $\omega_4 = 0.7 \pm 0.1$ kHz for the two-, three-, and four-body interactions, respectively. Since each of the resonant interactions scale differently with density, one could potentially fit simulations to the data to measure the Rydberg density of the sample.

Our experiment is a quantum quench [43,44]. We initially excite atoms to a many-body eigenstate of the Stark Hamiltonian at an electric field where they are noninteracting and then switch to the dipole-dipole interaction Hamiltonian by changing the field. The subsequent time evolution can be broadly divided into two outcomes.

The system can thermalize, eventually achieving an equilibrium state that can be specified with a small number of parameters. Or, in the case of many-body localization, the system fails to thermalize and retains a memory of its initial state [44–46]. Quenches have been used extensively to study both many-body localization and thermalization [25,46–49].

Since long-range dipole-dipole interactions should lead to efficient energy transport, one expects our system to thermalize. Indeed, for the two-body interaction this is what we seem to observe as the s-state fraction saturates near the expected level of 0.25. However, for the three-body and especially the four-body interactions, the saturation level is significantly lower than expected. This could indicate that the system fails to thermalize. In fact, Nandkishore and Sondhi have recently shown that many-body localization could be possible even in systems with long-range interactions [50].

To further investigate, we have extended our simulations of the four-body interaction to longer times and higher densities. The results show that the s-state fraction does not saturate at the expected value of 0.125. Távora *et al.* [51,52], suggest using the survival probability of the initial state as a criterion for numerically predicting thermalization. A rapidly decaying survival probability is a sign of thermalization as the memory of the initial state becomes inaccessible due to the spread of entanglement throughout the system. Our preliminary numerical analysis shows that the initial state survival probability in the four-body case does, indeed, decay significantly more slowly than for the two-body interaction.

We have presented experimental data showing the time dependence of few-body interactions in an amorphous ultracold sample of Rydberg atoms. While the matrix elements for the three- and four-body interactions are reduced because of the detuning, these interactions are stronger than one might expect because of the many paths from initial state to final state. The densities extracted from our simple model and our simulation differ by about a factor of 2 or 3, revealing the importance of always-resonant and beyond-nearest-neighbor interactions. Finally, the population transfer saturation levels suggest that the system may not thermalize as expected. Since the four-body resonance is relatively well separated from the two- and three-body peaks, it could prove useful for future experiments studying thermalization and localization.

This work was supported by the National Science Foundation under Grants No. 1607335 and No. 1607377.

[1] B. Yan, S. A. Moses, B. Gadway, J. P. C. Kaden, R. A. Hazzard, A..aria Rey, D. S. Jin, and J. Ye, Observation of dipolar spin-exchange interactions with lattice-confined polar molecules, Nature (London) **501**, 521 (2013).

[2] John L. Bohn, A. M. Rey, and J. Ye, Cold molecules: Progress in quantum engineering of chemistry and quantum matter, Science **357**, 1002 (2017).

[3] V. Efimov, Energy levels arising from resonant two-body forces in a three-body system, Phys. Lett. **33B**, 563 (1970).

[4] T. Kraemer, M. Mark, P. Waldburger, J. G. Danzl, C. Chin, B. Engeser, A. D. Lange, K. Pilch, A. Jaakkola, H.-C. Nägerl, and R. Grimm, Evidence for Efimov quantum states in an ultracold gas of caesium atoms, Nature (London) **440**, 315 (2006).

[5] C. H. Greene, P. Giannakeas, and J. Pérez-Ríos, Universal few-body physics and cluster formation, Rev. Mod. Phys. **89**, 035006 (2017).

[6] I. Ferrier-Barbut, H. Kadau, M. Schmitt, M. Wenzel, and T. Pfau, Observation of Quantum Droplets in a Strongly Dipolar Bose Gas, Phys. Rev. Lett. **116**, 215301 (2016).

[7] I. Ferrier-Barbut, M. Wenzel, F. Böttcher, T. Langen, M. Isoard, S. Stringari, and T. Pfau, Scissors Mode of Dipolar Quantum Droplets of Dysprosium Atoms, Phys. Rev. Lett. **120**, 160402 (2018).

[8] L. Tanzi, E. Lucioni, F. Famà, J. Catani, A. Fioretti, C. Gabbanini, R. N. Bisset, L. Santos, and G. Modugno, Observation of a Dipolar Quantum Gas with Metastable Supersolid Properties, Phys. Rev. Lett. **122**, 130405 (2019).

[9] W. R. Anderson, J. R. Veale, and T. F. Gallagher, Resonant Dipole-Dipole Energy Transfer in a Nearly Frozen Rydberg Gas, Phys. Rev. Lett. **80**, 249 (1998).

[10] I. Mourachko, D. Comparat, F. de Tomasi, A. Fioretti, P. Nosbaum, V. M. Akulin, and P. Pillet, Many-Body Effects in a Frozen Rydberg Gas, Phys. Rev. Lett. **80**, 253 (1998).

[11] B. Sun and F. Robicheaux, Spectral linewidth broadening from pair fluctuations in a frozen Rydberg gas, Phys. Rev. A **78**, 040701(R) (2008).

[12] B. G. Richards and R. R. Jones, Dipole-dipole resonance line shapes in a cold Rydberg gas, Phys. Rev. A **93**, 042505 (2016).

[13] I. Mourachko, Wenhui Li, and T. F. Gallagher, Controlled many-body interactions in a frozen Rydberg gas, Phys. Rev. A **70**, 031401(R) (2004).

[14] T. J. Carroll, S. Sunder, and M. W. Noel, Many-body interactions in a sample of ultracold Rydberg atoms with varying dimensions and densities, Phys. Rev. A **73**, 032725 (2006).

[15] E. A. Yakshina, D. B. Tretyakov, I. I. Beterov, V. M. Entin, C. Andreeva, A. Cinins, A. Markovski, Z. Iftikhar, A. Ekers, and I. I. Ryabtsev, Line shapes and time dynamics of the Forster resonances between two Rydberg atoms in a time-varying electric field, Phys. Rev. A **94**, 043417 (2016).

[16] V. Zhelyazkova and S. D. Hogan, Electrically tuned Förster resonances in collisions of NH_3 with Rydberg He atoms, Phys. Rev. A **95**, 042710 (2017).

[17] F. Jarisch and M. Zeppenfeld, State resolved investigation of Förster resonant energy transfer in collisions between polar molecules and Rydberg atoms, New J. Phys. **20**, 113044 (2018).

[18] W. R. Anderson, M. P. Robinson, J. D. D. Martin, and T. F. Gallagher, Dephasing of resonant energy transfer in a cold Rydberg gas, Phys. Rev. A **65**, 063404 (2002).

[19] S. Ravets, H. Labuhn, D. Barredo, L. Béguin, T. Lahaye, and A. Browaeys, Coherent dipole-dipole coupling between

two single Rydberg atoms at an electrically-tuned Förster resonance, Nat. Phys. **10**, 914 (2014).
[20] S. Ravets, H. Labuhn, D. Barredo, T. Lahaye, and A. Browaeys, Measurement of the angular dependence of the dipole-dipole interaction between two individual Rydberg atoms at a Förster resonance, Phys. Rev. A **92**, 020701 (R) (2015).
[21] C. S. E. van Ditzhuijzen, A. F. Koenderink, J. V. Hernández, F. Robicheaux, L. D. Noordam, and H. B. van Linden van den Heuvell, Spatially Resolved Observation of Dipole-Dipole Interaction between Rydberg Atoms, Phys. Rev. Lett. **100**, 243201 (2008).
[22] D. P. Fahey, T. J. Carroll, and M. W. Noel, Imaging the dipole-dipole energy exchange between ultracold rubidium Rydberg atoms, Phys. Rev. A **91**, 062702 (2015).
[23] J. L. Bigelow, J. T. Paul, M. Peleg, V. L. Sanford, T. J. Carroll, and M. W. Noel, Simulations of the angular dependence of the dipole–dipole interaction among Rydberg atoms, J. Phys. B **49**, 164003 (2016).
[24] F. Robicheaux and N. M. Gill, Effect of random positions for coherent dipole transport, Phys. Rev. A **89**, 053429 (2014).
[25] A. P. Orioli, A. Signoles, H. Wildhagen, G. Günter, J. Berges, S. Whitlock, and M. Weidemüller, Relaxation of an Isolated Dipolar-Interacting Rydberg Quantum Spin System, Phys. Rev. Lett. **120**, 063601 (2018).
[26] G. Kucsko, S. Choi, J. Choi, P. C. Maurer, H. Zhou, R. Landig, H. Sumiya, S. Onoda, J. Isoya, F. Jelezko, E. Demler, N. Y. Yao, and M. D. Lukin, Critical Thermalization of a Disordered Dipolar Spin System in Diamond, Phys. Rev. Lett. **121**, 023601 (2018).
[27] K. Xu, J.-J. Chen, Y. Zeng, Y.-R. Zhang, C. Song, W. Liu, Q. Guo, P. Zhang, D. Xu, H. Deng, K. Huang, H. Wang, X. Zhu, D. Zheng, and H. Fan, Emulating Many-Body Localization with a Superconducting Quantum Processor, Phys. Rev. Lett. **120**, 050507 (2018).
[28] J. Smith, A. Lee, P. Richerme, B. Neyenhuis, P. W. Hess, P. Hauke, M. Heyl, D. A. Huse, and C. Monroe, Many-body localization in a quantum simulator with programmable random disorder, Nat. Phys. **12**, 907 (2016).
[29] J. H. Gurian, P. Cheinet, P. Huillery, A. Fioretti, J. Zhao, P. L. Gould, D. Comparat, and P. Pillet, Observation of a Resonant Four-Body Interaction in Cold Cesium Rydberg Atoms, Phys. Rev. Lett. **108**, 023005 (2012).
[30] R. Faoro, B. Pelle, A. Zuliani, P. Cheinet, E. Arimondo, and P. Pillet, Borromean three-body FRET in frozen Rydberg gases, Nat. Commun. **6**, 8173 (2015).
[31] D. B. Tretyakov, I. I. Beterov, E. A. Yakshina, V. M. Entin, I. I. Ryabtsev, P. Cheinet, and P. Pillet, Observation of the Borromean Three-Body Förster Resonances for Three Interacting Rb Rydberg Atoms, Phys. Rev. Lett. **119**, 173402 (2017).
[32] I. I. Beterov, I. N. Ashkarin, E. A. Yakshina, D. B. Tretyakov, V. M. Entin, I. I. Ryabtsev, P. Cheinet, P. Pillet, and M. Saffman, Fast three-qubit Toffoli quantum gate based on three-body Förster resonances in Rydberg atoms, Phys. Rev. A **98**, 042704 (2018).
[33] I. I. Ryabtsev, I. I. Beterov, D. B. Tretyakov, E. A. Yakshina, V. M. Entin, P. Cheinet, and P. Pillet, Coherence of three-body Förster resonances in Rydberg atoms, Phys. Rev. A **98**, 052703 (2018).
[34] V. C. Gregoric, X. Kang, Z. C. Liu, Z. A. Rowley, T. J. Carroll, and M. W. Noel, Quantum control via a genetic algorithm of the field ionization pathway of a Rydberg electron, Phys. Rev. A **96**, 023403 (2017).
[35] V. C. Gregoric, J. J. Bennett, B. R. Gualtieri, A. Kannad, Z. C. Liu, Z. A. Rowley, T. J. Carroll, and M. W. Noel, Improving the state selectivity of field ionization with quantum control, Phys. Rev. A **98**, 063404 (2018).
[36] V. C. Gregoric, J. J. Bennett, B. R. Gualtieri, H. P. Hastings, A. Kannad, Z. C. Liu, M. R. Rabinowitz, Z. A. Rowley, M. Wang, L. Yoast, T. J. Carroll, and M. W. Noel, Perturbed field ionization for improved state selectivity, J. Phys. B **53**, 084003 (2020).
[37] U. F. Edgal and J. D. Wiley, Near-neighbor configuration and impurity-cluster size distribution in a Poisson ensemble of monovalent impurity atoms in semiconductors, Phys. Rev. B **27**, 4997 (1983).
[38] S. Chandrasekhar, Stochastic problems in physics and astronomy, Rev. Mod. Phys. **15**, 1 (1943).
[39] K. C. Younge, A. Reinhard, T. Pohl, P. R. Berman, and G. Raithel, Mesoscopic Rydberg ensembles: Beyond the pairwise-interaction approximation, Phys. Rev. A **79**, 043420 (2009).
[40] A. Cournol, J. Robert, P. Pillet, and N. Vanhaecke, Accurate density measurement of a cold Rydberg gas via non collisional two-body transitions, New J. Phys. **20**, 073042 (2018).
[41] D. Barredo, H. Labuhn, S. Ravets, T. Lahaye, A. Browaeys, and C. S. Adams, Coherent Excitation Transfer in a Spin Chain of Three Rydberg Atoms, Phys. Rev. Lett. **114**, 113002 (2015).
[42] T. J. Carroll, K. Claringbould, A. Goodsell, M. J. Lim, and M. W. Noel, Angular Dependence of the Dipole-Dipole Interaction in a Nearly One-Dimensional Sample of Rydberg Atoms, Phys. Rev. Lett. **93**, 153001 (2004).
[43] A. Polkovnikov, K. Sengupta, A. Silva, and M. Vengalattore, Colloquium: Nonequilibrium dynamics of closed interacting quantum systems, Rev. Mod. Phys. **83**, 863 (2011).
[44] D. A. Abanin and Z. Papić, Recent progress in many-body localization, Ann. Phys. (Amsterdam) **529**, 1700169 (2017).
[45] R. Nandkishore and D. A. Huse, Many-Body Localization and Thermalization in Quantum Statistical Mechanics, Annu. Rev. Condens. Matter Phys. **6**, 15 (2015).
[46] D. A. Abanin, E. Altman, I. Bloch, and M. Serbyn, Colloquium: Many-body localization, thermalization, and entanglement, Rev. Mod. Phys. **91**, 021001 (2019).
[47] A. Lukin, M. Rispoli, R. Schittko, M. E. Tai, A. M. Kaufman, S. Choi, V. Khemani, J. Léonard, and M. Greiner, Probing entanglement in a many-body–localized system, Science **364**, 256 (2019).
[48] J. Sous and E. Grant, Possible Many-Body Localization in a Long-Lived Finite-Temperature Ultracold Quasineutral Molecular Plasma, Phys. Rev. Lett. **120**, 110601 (2018).
[49] J. Sous and E. Grant, Many-body physics with ultracold plasmas: Quenched randomness and localization, New J. Phys. **21**, 043033 (2019).

[50] R. M. Nandkishore and S. L. Sondhi, Many-Body Localization with Long-Range Interactions, Phys. Rev. X **7**, 041021 (2017).

[51] M. Távora, E. J. Torres-Herrera, and L. F. Santos, Inevitable power-law behavior of isolated many-body quantum systems and how it anticipates thermalization, Phys. Rev. A **94**, 041603(R) (2016).

[52] M. Távora, E. J. Torres-Herrera, and L. F. Santos, Power-law decay exponents: A dynamical criterion for predicting thermalization, Phys. Rev. A **95**, 013604 (2017).